Systematic and random errors in self-mixing measurements: effect of the developing speckle statistics

Silvano Donati[1,2,*] and Giuseppe Martini[1]

[1]Department of Industrial and Information Engineering, University of Pavia, 27100 Pavia, Italy

[2]Graduate Institute of Precision Engineering, National Chung Hsing University, Taichung, China

*Corresponding author: silvano.donati@unipv.it

Received 3 March 2014; revised 27 April 2014; accepted 10 June 2014;
posted 11 June 2014 (Doc. ID 207459); published 22 July 2014

We consider the errors introduced by speckle pattern statistics of a diffusing target in the measurement of large displacements made with a self-mixing interferometer (SMI), with sub-λ resolution and a range up to meters. As the source on the target side, we assume a diffuser with randomly distributed roughness. Two cases are considered: (i) a developing randomness in z-height profile, with standard deviation σ_z, increasing from $\ll\lambda$ to $\gg\lambda$ and uncorrelated spatially (x, y), and (ii) a fully developed z-height randomness ($\sigma_z \gg \lambda$) but spatially correlated with various correlation sizes $\rho_{x,y}$. We find that systematic and random errors of all types of diffusers converge to that of a uniformly illuminated diffuser, independent of the actual profile of radiant emittance and phase distribution, when the standard deviation σ_z is increased or the scale of correlation $\rho_{x,y}$ is decreased. This convergence is a sign of speckle statistics development, as all distributions end up with the same errors of the fully developed diffuser. Convergence is earlier for a Gaussian-distributed amplitude than for other spot distributions. As an application of simulation results, we plot systematic and random errors of SMI measurements of displacement versus distance, for different source distributions standard deviations and correlations, both for intra- and inter-speckle displacements.

OCIS codes: (120.3180) Interferometry; (120.6165) Speckle interferometry, metrology.
http://dx.doi.org/10.1364/AO.53.004873

1. Introduction

The laser interferometer (LI) is a well-known instrument [1] capable of measuring displacements up to several meters with submicrometer resolution, and this remarkable performance makes it unique in a number of applications [1–5], like machine-tool positioning and dimensional control. The remote target is usually [1,2] a cooperative retroreflector (that is, a corner cube) positioned on one arm of the optical interferometer external to the laser source (usually a Michelson configuration with corner cube reflectors, as in Fig. 1).

In measuring a displacement from z_1 to z_2, the LI reads a phase $\Delta\phi = k(z_1 - z_2) + \phi_r$, where $k = 2\pi/\lambda$ is the wavenumber and ϕ_r is the phase error coming from a number of sources, like cyclic error and quantum noise [1]. Usually, we try to make $\phi_r \ll 1$ so that the error can be neglected in the digital readout mode of operation implemented by counting half-wavelength increments. In this mode, the corner cube retroreflector is useful in reducing detected signal attenuation and wavefront errors and also in avoiding disturbing backreflections, all at the expense of some invasiveness and constraint of operation, because the corner cube shall be mounted on the moving target and kept clean in the contaminant-rich (oil-drops, particulate) ambient of the typical mechanical workshop.

1559-128X/14/224873-08$15.00/0

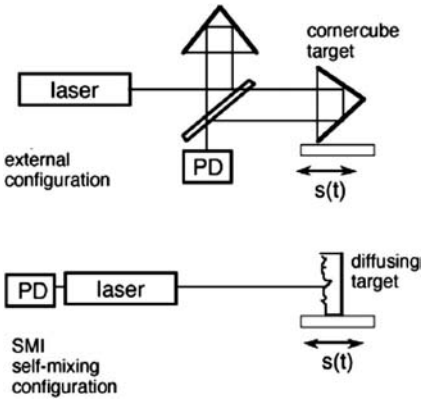

Fig. 1. Configuration of the conventional LI (top) based on the Michelson optical interferometer external to the laser source and the self-mixing interferometer (bottom) based on the modulations induced by the field injected back into the laser cavity, one requiring no optical components external to the laser.

Recently, a new configuration has been considered by several researchers for noninvasive operation of the LI, based on the self-mixing interferometer (SMI) [5].

The SMI does not require any optical component external to the laser (nor the optical interferometer), see Fig. 1, and, more importantly, it can also work well on a plain diffuser surface (like white paint or a metal finish), thus lifting the invasiveness of the corner cube.

However, working on a diffusing surface destroys the spatial coherence of the beam (Fig. 2) and gives rise to the speckle-pattern statistics [1–3,6–14] in the returning field being measured. As a consequence, an error is introduced in the phase shift read by the interferometer. The phase can now be written as

$$\Delta\phi = k(z_2 - z_1) + \phi_{\mathrm{sys}} + \phi_{\mathrm{rn}},$$

where ϕ_{sys} and ϕ_{rn} are the systematic and random errors introduced by the diffusing target, due to wavefront curvature of the source and to the roughness of the diffuser, respectively.

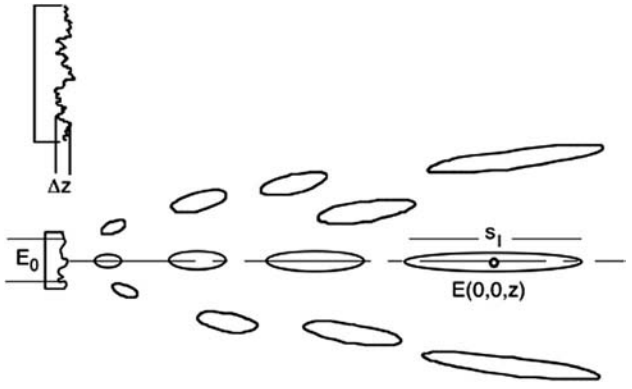

Fig. 2. Schematic representation of the speckle pattern field produced by a diffusing surface with a roughness depth $\Delta z \gg \lambda$ and a short-scale spatial correlation, and of the cigar-shaped speckles, the regions of coherence resulting from the diffuser statistics. Speckles point outward and their longitudinal length s_l increases with distance z. To model the SMI operating under speckle conditions, we consider the on-axis speckle field $E(0,0,z)$.

In previous papers [15,16] we have reported on the experimental performance of an SMI LI operating on a diffusing surface and found that displacements up to a few meters can be measured on noncooperative targets.

More recently, in [17] we analyzed theoretically the systematic and random errors, both for intra- and inter-speckle displacements, that is, for an on-axis displacement $z_2 - z_1$, either smaller or larger than the speckle longitudinal size s_l (Fig. 2), and we have shown that a sizeable span ($z_2 - z_1$ up to 1 m) can indeed be measured on a diffusing target with a small error (a few λs).

But, there were several assumptions in our analytical derivations: (i) the source was assumed an aperture with constant amplitude $E(x,y) = E_0 =$ constant for the calculation of the wavefront curvature giving the systematic error, and (ii) a fully developed speckle [6,7,11] was tacitly assumed for analyzing the random error.

A fully developed speckle is when the diffuser introduces a local phase $\phi_{\mathrm{diff}}(x,y) = k\Delta z(x,y) \gg 2\pi$ with a δ-like correlation $\rho = \langle \phi_{\mathrm{diff}}(x,y)\phi^*_{\mathrm{diff}}(x',y')\rangle = \delta(x-x',y-y')$, that is, a white noise spatial randomness (or near-field spatial incoherence at the source) [9]. As a deviation from ideality, we may take as an input to simulations two possible models: (i) an incompletely developed phase $k\Delta z$ (height profile randomness, case HPR), one not $\gg 2\pi$ but still with δ-like spatial correlation, and (ii) a developed phase $k\Delta z \gg 2\pi$ but with finite correlation on a dimension $\rho_{x,y}$ (spatially correlated roughness, case SPR).

Another assumption of [17] for the inter-speckle analysis of the random error was (iii) a quadratic sum of contributions, each equal to $\pi^2/3$ (the variance of a uniform distribution on $-\pi \ldots +\pi$) for the total phase variance, when the displacement $z_2 - z_1 > s_l$ encompasses several longitudinal speckles.

While these assumptions are quite reasonable and the results describe the experimental trends fairly well, they represent only the limited case of an ideal diffuser, or fully developed Gaussian statistics, which deviates appreciably from the statistics of a real diffuser, as already noted in [6–8] in general, and specifically in [15] with reference to the field amplitude distribution.

In addition, the disk-like amplitude distribution assumed for the source is not quite matched by real, Gaussian or Gaussian-polynomial modes emitted by a laser. So, we argued that it may be interesting to find out how fast the statistics of the nonideal diffuser converges to that of the ideal case at increasing surface randomness, or how the developing speckle statistics plays a role in converging asymptotically to the ideal case.

In this paper, we present results of simulations aimed to clarify the above points. Simulations have been carried out by numerical calculation of the on-axis field $E(0,0,z) = E_0 \exp i\phi(z)$ and then of the

systematic and random phase errors generated in the on-axis displacement $z_2 - z_1$ measured by an LI, as a function of distance z. As a realistic choice for measurements, z is assumed to range from 0.01 to 2 m (in 1000 steps), with $\lambda = 1$ μm, and the source diameter is taken as $D = 1$ mm. The source is subdivided into 1 μm by 1 μm elemental areas, to each of which a random phase $k\Delta z$ is attributed, picked from the selected random distribution (e.g., uniform in $-\pi$ to $+\pi$ or Gaussian with variance σ^2_{diff}). The phase associated with each area is uncorrelated with the neighboring areas, in the first case, of all-vertical (or height) randomness (HPR). In the second case, we repeat the calculations after introducing a spatial correlation on the random outcomes $k\Delta z$ of individual areas. This is done by attributing a phase given by the weighted sum of phases in N_a adjacent areas. This is the case of spatial (or in-plane) randomness or SPR.

We carry out calculations of the phase variance (Section 2) for several amplitude distributions of the source, namely, disk, Gaussian, and Gaussian–Laguerre (to model an LP01 mode), and for several source phase distributions, uniform with different widths up to $-\pi \ldots + \pi$ and Gaussian with different standard deviations σ up to several π.

Results presented in next sections first of all confirm the theoretical trends found in [17]. They also show that, irrespective of the starting amplitude distribution, the systematic error converges to the analytical result of the rectangular aperture (constant amplitude and constant phase) when the speckle is fully developed. Also, the theoretical random error of the rectangular aperture with uniformly distributed (in $-\pi$ to $+\pi$) random phase is approached by all distributions at increasing phase roughness of the source, with some deviation for large distance, when z becomes smaller than the speckle size s_l and the trend of intra-speckle random error is ultimately followed.

2. Systematic and Random Errors

We carried out our numerical simulations starting from the Fresnel–Huygens approximation for the propagation of field E, from the source plane ξ, η at $z = 0$, to the receiver plane x, y placed at a distance z

$$E(x,y,z) = (1/\lambda z)\exp ikz \exp[ik(x^2+y^2)/2z] \times \iint_{-\infty,+\infty} d\xi d\eta E_S(\xi,\eta)\exp[ik(\xi^2+\eta^2)/2z] \times \exp[-ik(x\xi+y\eta)/z]\exp i\phi_{\text{diff}}(\xi,\eta), \quad (1)$$

where symbols have the usual meaning, $E_S(\xi,\eta)$ is the source in which we include an eventual deterministic phase $\exp[i\phi_S(\xi,\eta)]$, and $\phi_{\text{diff}}(\xi,\eta) = k\Delta z(\xi,\eta)$ is the random phase distribution due to the roughness profile Δz (Fig. 2).

From Eq. (1), with $E_S(\xi,\eta) = E_{S0} =$ constant inside a circle of diameter D, we find [1,8,11] for the longitudinal speckle size (Fig. 2)

$$s_l = \lambda(2z/D)^2, \quad (2)$$

and write the on-axis field $E(0,0,z)$ received at distance z by the LI (or SMI) instrument (Fig. 2) as

$$E(0,0,z) = E_0(z)\exp i\Psi(z) = E_0(z)\exp i[kz + \phi_{\text{sys}} + \phi_{\text{rn}}], \quad (1A)$$

where ϕ_{sys} is the systematic phase contribution added to the propagation term kz, and ϕ_{rn} is the random error contribution, which has zero mean and variance $\langle\delta\phi^2_{\text{rn}}\rangle = \sigma^2_{\text{rn}}$ on the set of $\phi_{\text{diff}}(\xi,\eta)$ random outcomes describing the surface roughness.

We then apply to the measured $\Psi(z)$ a systematic phase correction, SPC, and obtain the displacement as

$$z_2 - z_1 = [\Psi(z_2) - \Psi(z_1) - \text{SPC}]/k, \quad (3)$$

where

$$\text{SPC} = -[\phi_{\text{sys}}(z_1) - \phi_{\text{sys}}(z_2)]. \quad (3A)$$

The term ϕ_{sys} can be calculated analytically from Eq. (1) for $\phi_{\text{diff}} = 0$, that is, for a simple aperture source of diameter D, that is one that has $E_0(\xi,\eta) = E_{S0}$ for $\xi^2 + +\eta^2 < (D/2)^2$, and $\phi_{\text{diff}} = 0$ for $\xi^2 + + \eta^2 > (D/2)^2$.

This is a reference case and we call it circular aperture constant phase (CA-CP). As in [17], we get from Eq. (1) with easy calculations

$$\phi_{\text{sys}} = kD^2/16z, d\phi_{\text{sys}}/dz = -kD^2/16z^2, \quad (4)$$

and for a displacement from z_1 to z_2 the phase correction is

$$\text{SPC} = \int_{z1\ldots z2}(d\phi_{\text{sys}}/dz)dz = (kD^2/16)(1/z_2 - 1/z_1) \approx -(kD^2/16z^2)\Delta_{12}, \quad (5)$$

where we have introduced $\Delta_{12} = z_2 - z_1$ and assumed $\Delta_{12} \ll z_1, z_2$ in the last term.

This result is the benchmark for developing speckle, and we plot $d\phi_{\text{sys}}/dz = kD^2/16z^2$ as a red line in all figures of systematic error to follow.

Another analytical result useful as reference is the systematic error of a Gaussian-distributed amplitude (GA-CP) source, with no phase error ($\sigma^2_{\text{rn}} = 0$), basically a fundamental Gaussian mode starting to propagate from $z = 0$. In this case, Eq. (1) gives, for a Gaussian with spot size w_0

$$\phi_{\text{sys}} = a\tan[kw_0^2/2z], \quad (6A)$$

$$d\phi_{\text{sys}}/dz = -(kw_0^2/2z^2)/[1 + (kw_0^2/2z)^2]. \quad (6B)$$

A formulation equivalent to Eq. (6A) was derived in [18].

To have Eqs. (5) and (6) coincide in the far-field, for $z \gg kw_0^2/2$, we shall assume $w_0 = D/2\sqrt{2}$. With this choice, we plot Eq. (6) in all the figures to follow as a green line.

Turning now to the random phase error ϕ_{rn}, we have two cases, according to whether the displacement $z_2 - z_1$ is smaller or larger than the speckle longitudinal size s_l. In the first case, we call it intra-speckle, the rms error σ_{rn} is found [17] as

$$\begin{aligned}\sigma_{\mathrm{rn(intra)}} &= (\pi C/2\sqrt{2})(D/2)^2/\lambda z^2 \Delta_{12} \\ &= (\pi C/2\sqrt{2})\Delta_{12}/s_l, \end{aligned} \tag{7}$$

where C is a factor not much different from unity, as calculated in [8]. Second, when the pass from one speckle to the next because $z_2 - z_1 > s_l$ we are in the inter-speckle case. Using a straightforward argument of statistical variables propagation, in [17] we have found that the rms error is then

$$\begin{aligned}\sigma_{\mathrm{rn(inter)}} &= -\sqrt{(\pi/24)}k^{1/2}D(1/z_2 - 1/z_1)^{1/2}, \\ &\quad \text{and for } \Delta_{12} \ll z_{1,2} \\ &\approx (\pi/\sqrt{3})(D/2z)\sqrt{(\Delta_{12}/\lambda)} = (\pi/\sqrt{3})(\Delta_{12}/s_l)^{1/2}. \end{aligned} \tag{8}$$

Comparing Eqs. (7) and (8), we see that internal to a speckle the error is about the ratio Δ_{12}/s_l of displacement to (longitudinal) speckle size, whereas for large displacement extending outside the speckle size, the error increases with the square root of the ratio Δ_{12}/s_l (or number of speckles crossed along the displacement). As the multiplicative factors in Eqs. (7) and (8) do not differ much (it is $\pi/\sqrt{3} = 1.81$ and $\pi C/2\sqrt{2}$ ranges typically from 2.2 to 4.5) the break point between intra- and inter-speckle errors is found by equating the terms Δ_{12}/s_l and $(\Delta/s_l)^{1/2}$ resulting in the condition $\Delta_{12} = s_l$, or

$$\Delta_{12} = (D/2)^2/\lambda. \tag{9}$$

This result is simple, yet not trivial, as it tells us that Eqs. (7) and (8) are the piecewise asymptotic approximation of the speckle error for $\Delta_{12} < s_l$ and $\Delta_{12} > s_l$, or, for any value of displacement Δ_{12}.

3. Results of Simulations

A. HPR Case

Several combinations of amplitude $E(\xi,\eta)$ and phase $\phi_{\mathrm{diff}}(\xi,\eta)$ distributions in shape have been considered to characterize the case of height profile randomness (HPR), as follows.

In amplitude

(i) circular aperture (acronym CA), or disk-like field distribution, with $E_S(\xi,\eta) = E_{S0}$ inside a diameter D, and $E_S(\xi,\eta) = 0$ outside;

(ii) Gaussian field amplitude distribution (acronym GA), with $E_S(\xi,\eta) = E_{S0}\exp -(\xi^2+\eta^2)/w^2$; and

(iii) higher-order mode, e.g., Gaussian–Laguerre LP_{01} distribution (acronym GL).

In phase

(i) constant phase with no random part, $\phi_{\mathrm{diff}}(\xi,\eta) = 0$, (acronym CP) corresponding to free propagation through a circular aperture or of a Gaussian mode (for the CA and GA above);

(ii) random with uniform (or rectangular) phase distribution in the interval $-K\pi < \phi_{\mathrm{diff}}(\xi,\eta) < K\pi$ (acronym RP), where K is the speckle-developing parameter ($K \ll 1$ for undeveloped speckle, and $K = 1$ for fully developed speckle); and

(iii) random phase with Gaussian distribution and rms standard deviation $\sigma_{\mathrm{diff}} = K\pi$ (acronym GP), where K is the parameter regulating the speckle development.

Systematic error. Results of simulations of the systematic error derivative, $d\phi_{\mathrm{sys}}/dz$, see Eqs. (4) and (6), are plotted in Figs. 3 and 4 along with the results for CA-CP [circular aperture constant phase, see Eq. (4)] and the GA-CP [Gaussian diffracting mode, see Eq. (5)]. In Fig. 3 we plot the case of circular aperture, Gaussian phase, CA-GP for several values of rms phase $\sigma = K\pi$, with $K = 0.1$, 0.3, 0.5, 1.0. 2.0, and 5.0. As can be seen, the diagrams are all nearly coincident (except for small numerical fluctuations) to the CA-CP case, implying that phase distribution has a weak influence on the systematic error. The same behavior (not reported here for

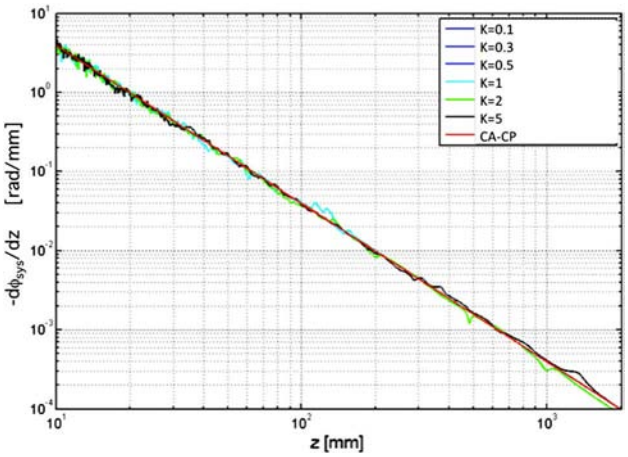

Fig. 3. Effect of the random phase distribution on the derivative $d\phi_{\mathrm{sys}}/dz$ of the systematic error, plotted versus distance z from 10 to 2000 mm. The red line is the asymptotic curve for a circular (or disk) aperture with constant phase (CA-CP). Superposed to it are the results for some HPR cases: a CA-GP, circular aperture with a Gaussian-distributed random phase and standard deviation $\sigma = K\pi$ with $K = 0.1$, 0.3, 0.5, 1.0, 2.0, and 5.0. All the CA-GP at different K are nearly coincident to the disk-aperture case even at small K. Not shown in figure, also CA-RP and GA-GP at high K are well-superposed to the CA-GP curve. The source has a diameter $D = 1$ mm, and the wavelength is 1 μm.

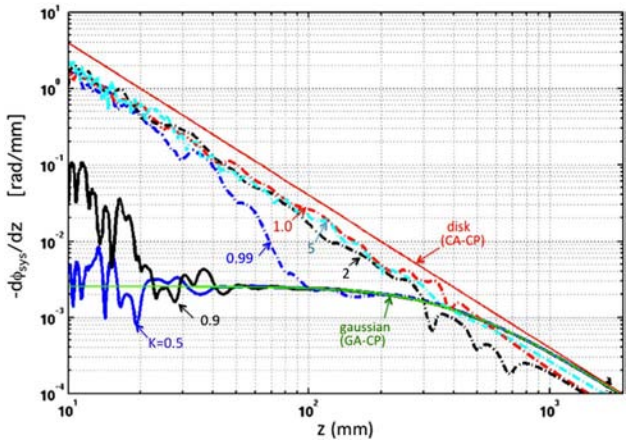

Fig. 4. HPR case. The effect of the diffuser amplitude and phase distribution on the derivative $d\phi_{sys}/dz$ of the systematic error, plotted versus distance z. Two asymptotic curves are indicated: for a disk aperture (CA-CP), red line, and for a Gaussian mode GA-CP, green line. Intermediate curves are for the GA-GP source, with Gaussian amplitude distribution and Gaussian random phase with rms $\sigma = K\pi$ and $K = 0.5$, 0.9, 0.99, 1.0. 2.0, and 5.0. The curves start from GA-CP at small K and end on the CA-CP for K approaching unity. The shift downward (of ≈2) of the GA-GP $K > 1$ curves with respect to CA-CP is due to spot size w_0 normalization. The source has a diameter $D = 1$ mm, and the wavelength is $\lambda = 1$ μm.

brevity) was also observed for the cases CA-RP and GL-CP.

Figure 4 shows the curves for a GA-GP source, for several values of K (0.5, 0.9, 0.99, 1.0, 2.0, and 5.0). In this case, the distributions start from close to the GA-CP curve at small K and gradually reach up to the CA-CP curve as K is increased (the factor of 2 difference in amplitude is because size w_0 of the GA is equivalent to $D/2\sqrt{2}$ of the RA). Convergence is a clear sign of speckle statistics becoming developed.

From this point of view, we see that for up to $K \approx 0.5$ the added Gaussian noise has not changed the error much with respect to the undisturbed (freely propagating Gaussian) and that the final error trend of the circular aperture (indicating full speckle development) is reached at $K \approx 1$.

As seen from Figs. 3 and 4, for $K = 1$ (at large diffuser phase) the systematic error of the Gaussian GA-GP is the same of CA-GP, a rectangular amplitude with random phase, and both deviate very little from the curve of the circular aperture CA-CP.

This feature suggests that the phase statistics predominate over amplitude distribution statistics in setting the systematic error.

A qualitative explanation for this feature is presented in Fig. 5. Consider point P of the Gaussian (dotted line) source: if the field exiting from P is given a random phase between $-\pi$ and π, this is the same as if point P were moved up or down to P' and P'', where phase kz differs by $-\pi$ and π.

This is a sort of spatial convolution of the initial Gaussian distribution with a rectangular point spread function (lines a and b), and the result is a

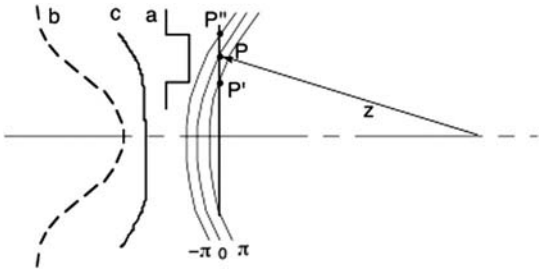

Fig. 5. Because of the random phase $-\pi$ to π added by the diffuser, it is like each point P is spread up/down to P' and P'' (line a), and this is a convolution of the initial Gaussian (dotted line b) to end as an almost rectangular distribution (line c)

flattening of the initial distribution to a uniform one, asymptotically.

For the same reason, the $d\phi_{sys}/dz$ distribution of a rectangular amplitude (constant E_S) with Gaussian phase, or CA-GP, is practically coincident with the red line of CA-CP for $K = 0.1$ and does not deviate any more for $K = 0.3$–0.5–1–2–5.

To extend the comparison, we calculated the $d\phi_{sys}/dz$ for an LP01 mode, GL-GP, and found that the results (not reported in this paper for conciseness) are once again similar to those of the CA-CP, except for a scale factor of ≈3, due to the larger effective spot size of the mode.

In conclusion, the systematic error and its correction SPC tends asymptotically to that of a rectangular diffraction aperture (CA-CP) at the increase of the phase randomness attributed to each elemental area of the source spot. The trend is largely independent of the exact amplitude distribution, whereas convergence of $d\phi_{sys}/dz$ to CA-CP is faster with the increase of diffuser phase variance σ^2_{dif}.

A comment about numerical oscillations and small spikes appearing in the computed results: they are due to (i) the finite size (1000 individual samples) chosen in the simulations as a reasonable compromise between computing time and smoothness of the results, and (ii) the discretization on distance z intervals, introducing spikes due to 2π-phase jumps. When spurious features are comparatively large, such as in Fig. 4 at small z (<50 mm), we make sure that the average trend of the curve is clearly visible.

Random error. The random phase error ϕ_{rn} of Eq. (1A) has been computed using the Fresnel–Huygens approximation [Eq. (1)] by the numerical simulation outlined in Sections 1 and 2. Care has been exercised such that no artifact is added in the final folding of phase in the interval $-\pi$ to $+\pi$, when computing phase differences of displacements from z_1 to z_2.

Two cases have been calculated in detail, CA-GP, with uniform amplitude and Gaussian random phase $\sigma = K\pi$, and GA-GP, with Gaussian amplitude and Gaussian random phase $\sigma = K\pi$.

In both cases, the errors follow the same trend with the speckle-developing parameter K, approaching the intra- or inter-speckle curve at increasing K, that is, when the speckle becomes developed. Also, other

combinations of amplitude and phase distributions have been checked in selected cases and follow essentially the same trend.

Thus, for sake of brevity, we report results for the GA-GP distributions only. Four values of displacements are considered: $\Delta_{12} = 0.2$ mm (of interest for vibration pickup), 2, 20, and 200 mm (of interest for displacement measurements) [12,13, 17].

In all the cases considered, the value of K at which the asymptotic curves are practically reached is 0.99–1.0, whereas at $K = 0.9$ (and 0.5) the rms error is already one (and ≈2) decade smaller.

B. SPR Case

Last, we consider the case of spatially correlated roughness (SPR) of a source with spatial correlation of the random height Δz in the plane x, y.

Correlation is introduced by sorting out the set of random phases Δz of the elemental area (1 μm by 1 -μm) array as above, and then computing for each area the linearly weighted sum of N_a adjacent phases, with N_a ranging from 0 (no correlation) to 100. Since the weight is assumed to linearly decrease with distance, the correlation radius ranges from 0 to ½100 = 50 μm. The amplitude of illumination is chosen as a Gaussian distribution, and the phase is also taken as Gaussian with $\sigma_{\text{diff}} = 5\pi$ (thus, a distribution almost uniform after the folding of phase in $-\pi \ldots + \pi$). This correlated case corresponds to a GA-GP source of Fig. 4 with $k = 5.0$.

In Figs. 7A and 7B we plot the systematic $d\phi_{\text{sys}}/dz$ and the random error ϕ_{rn}, respectively. A comparison of Fig. 7A with Fig. 4 readily reveals a striking similarity of trends in the two cases.

Indeed, in both diagrams we can see a nearly identical evolution from the undeveloped statistics (with $k = 0.5$–0.9 in Fig. 4 and with $N_a = 3$–10 in Fig. 7A) to the almost fully developed case ($K = 1$–5 in Fig. 4 and $N_a = 0$–100 in Fig. 7A).

The same similarity can be appreciated by comparing the random errors for a $\Delta_{12} = 20$ mm displacement, with either purely "white noise" height statistics (Fig. 6C) or spatial-correlation statistics (Fig. 7B).

From the application point of view, it is interesting to note that the uncertainty of the interferometric

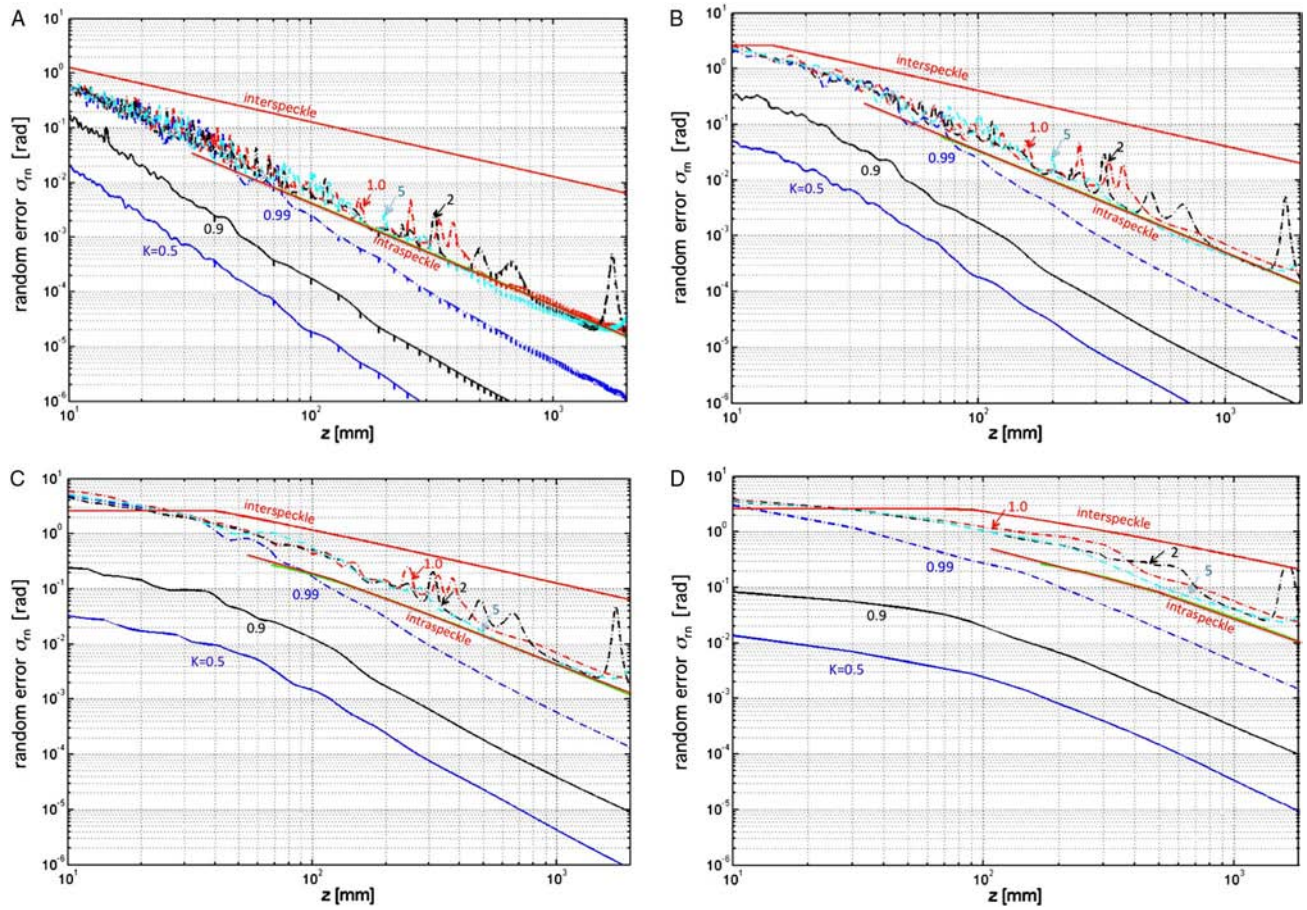

Fig. 6. A, HPR case. The random error σ_{rn} is plotted versus distance z for the inter- and intra-speckle cases [straight lines, Eqs. (7) and (8)] and the developing statistics of GA-GP, a Gaussian amplitude distribution and Gaussian random phase, with several values of standard deviation $\sigma_{\text{diff}} = K\pi$. Other values are as in Fig. 4. The displacement is $\Delta_{12} = 0.2$ mm. Oscillations and spikes are due to the finite sample size and to discretization. B, same as in A, for a displacement of $\Delta_{12} = 2$ mm. C, same as in A, for a displacement of $\Delta_{12} = 20$ mm. D, same as in A, for a displacement of $\Delta_{12} = 200$ mm.

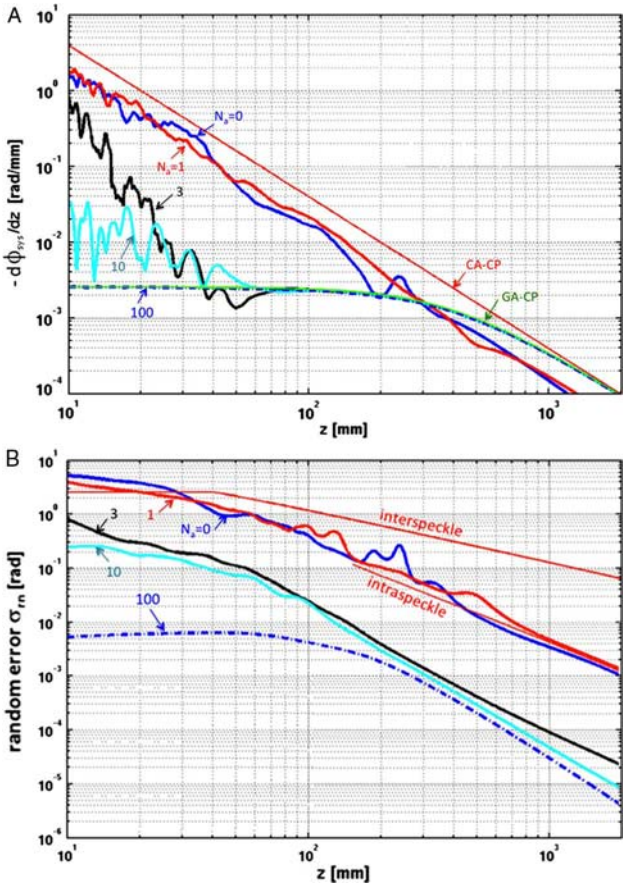

Fig. 7. A, SPR case. The derivative $d\phi_{\text{sys}}/dz$ of the systematic error, plotted versus distance z, for a GA-GP source, with Gaussian amplitude distribution and correlated Gaussian random phase with rms $\sigma = 5\pi$ and scale of correlation $N_a = 0$, 1, 3, 10, and 100. The two asymptotic curves CA-CP (red) and GA-CP (green) are as in Fig. 4. The source has a diameter $D = 1$ mm, and the wavelength is $\lambda = 1$ μm. B, SPR case. The random error σ_{rn} is plotted versus distance z for the inter- and intra-speckle cases [straight lines, Eqs. (7) and (8)] and the developing statistics of correlated GA-GP, a Gaussian amplitude distribution and Gaussian random phase, with a scale of correlation $N_a = 0$, 1, 3, 10, and 100. Displacement is $\Delta_{12} = 20$ mm. The ripple in the curves is due to numerical oscillations.

measurements made on a diffusing surface may reach values well below the fully developed case of speckle statistics.

Of course, to take advantage of this result, we shall first correct the systematic error, the amount of which may be much larger than the random error, especially when distance is large compared to spot size, as already pointed out in [17] (see Figs. 5 and 7), and we shall also ensure that detector noise is negligible [14].

4. Conclusions

The results of simulations on the developing speckle pattern statistics, which are new to the best of our knowledge, are in good agreement with the theory of the asymptotic case developed in [17].

A new finding is that, independent from the starting amplitude distribution of the source, the systematic error $\phi_{\text{sys}}(z)$ converges to the analytical result $\phi_{\text{sys-an}}(z)$ of the rectangular aperture source when the speckle is fully developed, also for distributions that start from a much different analytical dependence. The same conclusion holds for the random error ϕ_{rn}: the analytical result for the circular aperture (CA-CP) is approached by all distributions at increasing phase roughness of the source, or decreasing spatial correlation, with a clear passage from the intra-speckle to the inter-speckle analytical dependence when z becomes larger than the speckle size s_l.

Besides offering new insight into the fundamental properties of developing speckle pattern, our results are new and interesting in practical applications of LI as they provide an estimate of the effective error in the case of a diffuser deviating appreciably from the ideal case.

Appendix A: List of Acronyms

LI = laser interferometer
SMI = self-mixing interferometer
SPC = systematic phase correction
HPR = height profile randomness
SPR = spatially correlated roughness
CA = rectangular diffraction aperture (or disk-like aperture) no randomness
GA = Gaussian-distributed amplitude (or Gaussian mode) no randomness
intra-speckle = $s_l > z_2 - z_1$ displacement less than speckle size
intra-speckle = $s_l < z_2 - z_1$ displacement larger than speckle size
GL = Gaussian–Laguerre LP_{01} distribution
CP = uniform phase with no random part
RP = random rectangular distributed phase, in the interval $-K\pi < \phi_{\text{diff}}(\xi, \eta) < K\pi$
GP = random Gaussian-distributed phase with rms standard deviation $\sigma_{\text{diff}} = K\pi$

Work was performed within the framework of COST Action BM-1205.

References

1. S. Donati, *Electro-Optical Instrumentation* (Prentice Hall, 2004) Chap. 4.
2. S. Donati and S. Merlo, "Applications of diode laser feedback interferometry," J. Opt. **29**, 156–161 (1998).
3. G. Plantier, N. Servagent, A. Sourice, and T. Bosch, "Real-time parametric estimation of velocity using optical feedback interferometry," IEEE Trans. Instr. Meas. **50**, 915–919 (2001).
4. S. Donati and M. Norgia, "Self-mixing interferometry for biomedical signals sensing," IEEE J. Sel. Top. Quantum Electron., doi: 10.1109/JSTQE.2013.2270279M (in press).
5. S. Donati, "Developing self-mixing interferometry for instrumentation and measurements," Laser Photonics Rev. **6**, 393–417 (2012).
6. J. W. Goodman, *Speckle Phenomena in Optics: Theory and Applications*, 2nd ed. (Roberts, 2007).
7. J. Ohtsubo, "Statistical properties of differentiated partially developed speckle pattern," J. Opt. Soc. Am. **72**, 1249–1252 (1982).
8. S. Donati and G. Martini, "Speckle-pattern intensity and phase second-order conditional statistics," J. Opt. Soc. Am. **69**, 1690–1694 (1979).
9. J. Ohtsubo, "Joint probability density function of partially developed speckle patterns," Appl. Opt. **27**, 1290–1292 (1988).

10. P. Lehmann, "Surface-roughness measurement based on the intensity correlation function of scattered light under speckle-pattern illumination," Appl. Opt. **38**, 1144–1152 (1999).
11. C. J. Dainty, "The statistics of speckle pattern," in *Progess in Optics*, E. Wolf, ed. (North-Holland, 1976), Vol. **XIV**, pp. 1–44.
12. B. R. Masters, "Three-dimensional microscopic tomographic imagings of the cataract in a human lens in vivo," Opt. Express **3**, 332–338 (1998).
13. R. Atashkhooei, S. Royo, and F. J. Azcona, "Dealing with speckle effects in self-mixing interferometry measurements," IEEE Sens. J. **13**, 1641–1647 (2013).
14. S. Donati, *Photodetectors* (Prentice-Hall, 2000), Chap. 4.
15. M. Norgia, S. Donati, and D. d'Alessandro, "Interferometric measurements of displacement on a diffusing target by a speckle-tracking technique," IEEE J. Quantum Electron. **37**, 800–806 (2001).
16. M. Norgia and S. Donati, "A displacement-measuring instrument using self-mixing interferometry," IEEE Trans. Instrum. Meas. **52**, 1765–1770 (2003).
17. S. Donati, G. Martini, and T. T. ambosso, "Speckle pattern errors in self-mixing interferometry," IEEE J. Quantum Electron. **49**, 798–806 (2013).
18. A. Yariv and P. Yeh, *Photonics*, 6th ed. (Oxford University, 2007).